Binding Properties of the Stilbene Disulfonate Sites on Human Erythrocyte AE1: Kinetic, Thermodynamic, and Solid State Deuterium NMR Analyses†

Andrew M. Taylor,‡ Gerhard Gröbner, Philip T. F. Williamson, and Anthony Watts*

Biomembrane Structure Unit, Department of Biochemistry, Oxford University, South Parks Road, Oxford OX1 3QU, U.K.

Received March 17, 1999; Revised Manuscript Received June 15, 1999

ABSTRACT: A novel stilbene disulfonate, 4-trimethylammonium-4′-isothiocyanostilbene-2,2′-disulfonic acid (TIDS), has been chemically synthesized, and the interaction of this probe with human erythrocyte anion exchanger (AE1) was characterized. Covalent labeling of intact erythrocytes by [$N^+(^{14}CH_3)_3$]TIDS revealed that specific modification of AE1 was achieved only after removal of other ligand binding sites by external trypsinization. Following proteolysis, $(1.2 \pm 0.4) \times 10^6$ TIDS binding sites per erythrocyte could be blocked by prior treatment with 4,4′-diisothiocyanostilbene-2,2′-disulfonic acid (DIDS), a highly specific inhibitor of AE1. Inhibition of sulfate equilibrium exchange by TIDS in whole cells was described by a Hill coefficient of 1.10 ± 0.06, which reduced to 0.51 ± 0.01 following external trypsinization. The negative cooperativity of TIDS binding following external trypsinization suggests that trypsin-sensitive proteins modulate allosteric coupling between AE1 monomers. Thermodynamic analysis revealed that TIDS binding induces smaller conformational changes in AE1 than is observed following DIDS binding. The similar inhibitory potencies of both TIDS ($IC_{50} = 0.71 \pm 0.48$ μM) and DIDS ($IC_{50} = 0.2$ μM) imply that there is no correlation between the ability of stilbene disulfonates to arrest anion exchange function and the magnitude of ligand-induced conformational changes in AE1. Solid state ^2H NMR analysis of a [$N^+(CD_3)_3$]TIDS−AE1 complex in both unoriented and macroscopically oriented membranes revealed that large amplitude "wobbling" motions describe ligand dynamics. The data are consistent with a model where TIDS bound to AE1 is located exofacially in contact with the bulk aqueous phase.

The anion exchanger (AE) superfamily is responsible for chloride−bicarbonate electroneutral exchange in several types of biological membranes (*1*), of which the human erythrocyte AE1 (band 3) is the best characterized member (*2*). Stilbene disulfonates are a potent class of AE inhibitors that are specific for AE1 in intact erythrocytes and have been used to elucidate the kinetics of AE1-mediated chloride−bicarbonate exchange (*3*). The binding of these inhibitors to AE1 is biphasic, where initial fast association of the ligand with AE1 precedes a much slower ligand-induced conformational change in the protein (*4*, *5*). Fluorescence studies indicate that the slower ligand-induced conformational change in AE1 is concomitant with a relocation of the probes to a rigid, hydrophobic cleft within the interior of the protein and close to the cytoplasmic membrane surface (*6*, *7*). However, this model is not supported by the observations that (a) ascorbate quenched a spin-labeled stilbene disulfonate−AE1 complex only from the external surface of the bilayer (*8*), (b) the fluorescence lifetime of a stilbene disulfonate bound to AE1 was unaffected by labeling the protein cytoplasmic domain with a fluorescent acceptor (*9*), and (c) the isothiocyanate groups within a ligand−AE1 complex were found to be in contact with solute (*10*).

Although extensively used to study AE1 function, the mechanism of stilbene disulfonate inhibition is not completely resolved. A direct competition model is supported by chloride NMR line-broadening studies (*11*), by work with spin-labeled stilbene disulfonates (*12*), and by studies of the direct binding of stilbene disulfonates to whole cells (*13*). Conversely, both kinetic and site-directed mutagenesis investigations favor an allosteric model for AE1 inhibition by stilbene disulfonates (*10*, *14*). Although the spatial location of the anion channel awaits more detailed structural information than is available at the present time, the low-resolution structure reveals a putative central channel between two AE1 monomers (*15*). Perturbation of the monomer−monomer interface upon stilbene disulfonate binding may therefore provide an allosteric mechanism for inhibition. Indeed, monomeric AE1 is unable to bind stilbene disulfonates, suggesting that dimerization is a prerequisite for stilbene disulfonate binding (*16*). The negative cooperativity of inhibition observed for some stilbene disulfonates supports an allosteric model, although negative cooperativity also seems to be a function of ionic strength, buffer composition, and stilbene disulfonate structure (*4*, *5*, *8*, *17*).

In this study, we introduce a $N^+(CD_3)_3$ group at the 4 position on a stilbene disulfonate and specifically covalently label AE1 with this compound in native membranes. Solid state deuterium NMR analysis provides information about the dynamics of the inhibitor bound to AE1 (*18*). The ^2H

† This work was supported by BBSRC (Senior Fellowship to A.W. and a studentship to A.M.T.) and HEFCE under the 1997 JREI exercise.

* To whom correspondence should be addressed: Biomembrane Structure Unit, Department of Biochemistry, Oxford University, South Parks Road, Oxford OX1 3QU, U.K. Telephone: 44 1865 275268. Fax: 44 1865 275234. E-mail: awatts@bioch.ox.ac.uk.

‡ Current address: Department of Physiology, University of Alberta, Edmonton, Alberta, Canada T6G 2H7.

10.1021/bi990618p CCC: $18.00
Published on Web 08/05/1999

spectra of the quaternary ammonium group are sensitive to motions about both the C_3' and the C_3 motional axes, where the C_3' axis is defined as three-site exchange between the C−D bonds of the methyl groups and the C_3 axis defines three-site exchange between the methyl groups (*19*). If both a static quadrupole coupling constant for an aliphatic deuteron of 170 kHz (*20*) and rapid rotation ($\tau_c^{-1} > 10^7$ s^{-1}) about both motional axes are assumed, the value of $\Delta\nu_q$[1] may be determined according to

$$\Delta\nu_q = {}^3/_{16} \times 170(3\cos^2\theta_{CD} - 1)(3\cos^2\theta_{NC} - 1) \quad (1)$$

where θ_{CD} is the angle between the C−D bond and the C_3' axis and θ_{NC} similarly defines the angle between the N−C bond and the C_3 axis (*19*). For tetrahedral geometry, where $\theta_{CD} = \theta_{NC} = 70.5°$, a value for $\Delta\nu_q$ of 14 kHz may be calculated. Additional fast motions further average $\Delta\nu_q$, whereas slower motions on the intermediate time scale ($\tau_c^{-1} \sim 10^5-10^6$ s) lead to complex line shapes (*21*). While protein dynamics may be investigated with unoriented samples, ^{2}H NMR can also provide structural details for macroscopically oriented systems (*22*, *23*). However, purely structural information may only be deduced after detailed characterization of probe dynamics (*22*).

Investigation of the interaction of chemically diverse stilbene disulfonates with AE1 begins to define the chemical nature of the inhibitor site (*1*), as well as providing information about the mechanisms responsible for inhibition of AE1 function by these compounds (*24*). In this study, solid state ^{2}H NMR analysis of AE1 specifically labeled with a deuterated stilbene disulfonate, together with both kinetic and thermodynamic analyses, provides a detailed description of the ligand−AE1 complex and insight into the mechanism of AE1 inhibition by these compounds.

EXPERIMENTAL PROCEDURES

Materials. 4-Amino-4′-nitrostilbene-2,2′-disulfonic acid disodium salt was purchased from TCI (Tokyo, Japan). [^{14}C]-Methyl iodide was obtained from Amersham. [$^2H_3$]Methyl iodide and deuterium-depleted water were purchased from Aldrich. $Na_2{}^{35}SO_4$ was obtained from ICN Biomedicals Ltd. DIDS was purchased from Molecular Probes. Melinex sheets were obtained from Agar Scientific. All other chemicals were reagent grade or better.

Synthesis of 4-Trimethylammonium-4′-isothiocyanostilbene-2,2′-disulfonic Acid (TIDS). Starting from 4-amino-4′-nitrostilbene-2,2′-disulfonic acid disodium salt, we performed the synthesis of 4-acetamido-4′-aminostilbene-2,2′-disulfonic acid as previously described (*25*). Methylation of 4-acetamido-4′-aminostilbene-2,2′-disulfonic acid was achieved by adaptation of a general method for quaternization of amines (*26*). 4-Acetamido-4′-aminostilbene-2,2′-disulfonic acid (4.56 g, 10 mmol), 1,2,2,6,6-pentamethylpiperidine (3.1 g, 20 mmol), and methyl iodide (3.9 g, 30 mmol) were suspended in *N*,*N*-dimethylformamide (25 mL). After the mixture had been stirred overnight at room temperature in the dark, 6% *N*,*N*-dimethylformamide in acetone (340 mL) was added and the mixture refluxed (30 min). The remaining solid was washed with ice-cold methanol and crystallized from hot H_2O/methanol (1.96 g, 40%). The ^{14}C-methylated and deuterated analogues were synthesized using the same protocol by substitution of methyl iodide for [^{14}C]methyl iodide and [$^2H_3$]methyl iodide, respectively. Deprotection of the amino group was achieved by refluxing 4-trimethylammonium-4′-acetamidostilbene-2,2′-disulfonic acid (2 g, 4 mmol) overnight in 1 M HCl (100 mL). Upon cooling, the mixture was evaporated to dryness and the pure product crystallized from water (1.6 g, 80%). Conversion of the amine to an isothiocyanate (1.1 g, 80%) was achieved as previously described (*25*). The identity of the product was confirmed by both negative electrospray mass spectroscopy and solution NMR.

Characterization of [^{14}C]TIDS Binding to Whole Erythrocytes. Labeling of whole erythrocytes with [^{14}C]TIDS was performed on fresh blood (*27*). In a typical experiment, 10 mL of blood was pelleted (1000*g* for 5 min at 4 °C), the buff coat removed, and the sediment washed twice with phosphate buffer [155 mM phosphate (pH 9.5)]. Labeling was performed by incubation of the resuspended cells (2 h at 37 °C with 50% hematocrit) with [^{14}C]TIDS (100 μM). Unreacted radiolabeled ligand was removed by three washes with PBS containing 1% bovine serum albumin (1000*g* for 5 min at 4 °C), followed by two washes with PBS (1000*g* for 5 min at 4 °C). Proteolysis of intact erythrocytes was performed by addition of either trypsin or chymotrypsin (200 μg/mL) to a 20% hematocrit cell suspension in PBS (*28*). After incubation (37 °C for 2 h), the cells were washed three times in ice-cold PBS containing 2 mM PMSF and erythrocyte ghosts prepared as described previously (*29*). Electrophoresis was performed on 10% (w/v) acrylamide slab gels using the discontinuous buffer system (*30*). Proteins were visualized with Coomassie blue R-250, and radioactivity was detected using Kodak Biomax film.

Stoichiometry of TIDS Binding. The concentration of erythrocytes in fresh blood was determined by Coulter Counter measurement. The remainder of the sample (5 mL) was labeled with [^{14}C]TIDS (100 μM, 5.00×10^{11} dpm/mol) and treated with trypsin (200 μg/mL), and ghost membranes were prepared. The sample was then split into two equal volumes, one for determination of total inhibitor content and the other for determination of the amount of inhibitor associated with lipid. The first aliquot was solubilized with SDS (10% w/v) and the total amount of inhibitor bound to the membrane determined by β-scintillation spectroscopy. Lipid was extracted into an organic solvent as previously described (*31*), and the amount of inhibitor associated with lipid was determined by β-scintillation spectroscopy.

Inhibition Studies. Fresh blood (200 μL) was diluted into SBS (10% hematocrit), incubated (37 °C for 30 min), and pelleted (1000*g* for 5 min at 4 °C), and the process was repeated twice more to ensure complete replacement of

[1] Abbreviations: CSA, chemical shift anisotropy; Ch39, chymotryptic C-terminal cleavage product; Ch61, chymotryptic N-terminal cleavage product; τ_c, correlation time; $\Delta\nu_q$, deuterium quadrupole splitting; H_2-DIDS, 4,4′-diisothiocyano-1,2-diphenylethane-2,2′-disulfonic acid; DIDS, 4,4′-diisothiocyanostilbene-2,2′-disulfonic acid; GPA, glycophorin A; MOPS, 3-(*N*-morpholino)propanesulfonic acid; NIDS, 4-nitro-4′-isothiocyanostilbene-2,2′-disulfonic acid; PBS, 155 mM phosphate (pH 7.4); PMSF, phenylmethanesulfonyl fluoride; SBS, 107 mM Na_2SO_4, 10 mM MOPS, and 5 mM glucose (pH 7.4); TIDS, 4-trimethylammonium-4′-isothiocyanostilbene-2,2′-disulfonic acid; [$^2H_9$]TIDS, 4-trideuteriomethylammonium-4′-isothiocyanostilbene-2,2′-disulfonic acid; Tris buffer, 10 mM NaCl, 10 mM Tris, and 0.5 mM EDTA (pH 8); SDS, sodium dodecyl sulfate.

sulfate for chloride. The cells were resuspended (50% hematocrit) into a solution containing 1 part of SBS to 9 parts of sucrose buffer [300 mM sucrose and 10 mM MOPS (pH 7.4)], and $Na_2{}^{35}SO_4{}^{2-}$ (10 μCi) was added. After incubation (37 °C for 1 h), the cells were washed four times by centrifugation in ice-cold SBS (10000*g* for 10 s). To initiate efflux, packed cells (100 μL) were added to SBS (9.9 mL at 37 °C). Aliquots were taken at suitable time intervals and pelleted (10000*g* for 10 s at 4 °C), and the supernatant was assayed for $^{35}SO_4{}^{2-}$ by β-scintillation spectroscopy. Further samples of the cell suspension were treated with trichloroacetic acid (50% w/v), and counted to derive the total internal initial radioactivity. The rate constant k for sulfate efflux was calculated from the equation $k = \log[(C_{total} - C_t)/(C_{total} - C_0)]/t$ min^{-1}, where C_{total}, C_0, and C_t are the total initial counts, the count at time zero, and the count at time t, respectively. Inhibition experiments were performed by adding TIDS at defined concentrations to SBS, prior to initiation of $^{35}SO_4{}^{2-}$ efflux by addition of packed cells.

Calorimetric Analysis. Erythrocyte ghost membranes (150 μL), obtained after labeling whole cells with TIDS and subsequent proteolysis with external trypsin, were dispensed into Perkin-Elmer aluminum pans. The sample and reference pan, which contained an equivalent volume of aqueous PBS, were heated from 10 to 90 °C at a scan rate of 5 °C/min in a Perkin-Elmer DSC 7 scanning calorimeter equipped with an intracooler and a PC controller. Samples of ghost membranes and DIDS-labeled ghost membranes were treated with external trypsin prior to calorimetric analysis.

NMR Sample Preparation. Ghost membranes, prepared from whole erythrocytes labeled with [$^2H_9$]TIDS and incubated with external trypsin prior to lysis, were washed twice with Tris buffer prepared in deuterium-depleted water (5000*g* for 5 min at 4 °C) and resuspended to a total protein concentration of 4 mg/mL in the same buffer. Partially oriented membrane films were prepared by depositing ghost membranes (1 mL at a total protein concentration of 4 mg/mL; 90000*g* for 16 h at 4 °C) onto Melinex plates (8 mm × 8 mm) by the method of isopotential spinning (*32*). A removable isopotential ultracentrifuge cell for use with the Beckman SW-28 swinging bucket rotor was constructed on the basis of a previous design (*33*), except that polycarbonate material (which is resistant to deformation at high rotor speeds) replaced Delrin. Following centrifugation, the membrane films were partially dehydrated over a saturated $(NH_4)_2SO_4$ solution in deuterium-depleted water (18 °C for 12 h with 81% humidity). For ^2H NMR experiments, these oriented membrane films (25 plates) were assembled into parallel stacks within a 10 mm external diameter NMR tube. The level of sample hydration was maintained within the closed tube by a saturated $(NH_4)_2SO_4$ solution in deuterium-depleted water.

NMR Procedures. All static ^2H NMR spectra were acquired on a Bruker MSL 400 spectrometer at a deuterium frequency of 61.5 MHz using a quadrupole-echo pulse sequence with appropriate quadrature phase cycling (*34*). The width of the 90° pulse was 6 μs, and echo delay times of 35 μs and a recycle time of 300 μs were used with a 10 mm coil. T_1 measurements were recorded on a Bruker AMX 360 spectrometer using an inversion−recovery pulse sequence with a 90° pulse width of 3.5 μs, a recycle time of 150 ms, and a sample spinning frequency of 5 kHz. Static ^2H NMR line shape simulations were performed as described previously (*35*). ^{31}P NMR spectra were acquired with broadband ^1H decoupling (25 kHz) on a Bruker MSL 400 spectrometer at a phosphorus frequency of 161 MHz, using a $^1/_2$ Hahn-echo pulse sequence with appropriate phase cycling. The width of the 90° pulse was 6 μs, and echo delay times of 30 μs and a recycle time of 3 s were used with a 10 mm coil. Chemical shifts were assigned relative to external 85% H_3PO_4. The quality of the orientation was assessed by using a line shape simulation algorithm based on previously described methods (*36*).

Other Methods. Protein concentrations were determined by the modified Lowry method (*37*). Thin sections of oriented membranes were prepared by fixing in buffered osmium tetroxide, processed by standard procedures for thin sectioning, and visualized using a JEOL 2000 EX electron microscope with an accelerator voltage of 100 keV.

RESULTS

Labeling of Intact Erythrocytes with [^{14}C]TIDS. Covalent labeling of intact erythrocytes by [^{14}C]TIDS was investigated by polyacrylamide gel electrophoresis (Figure 1). Panel a shows the densitometric scan derived from a Coomassie Blue-stained gel of erythrocyte membranes (lane 1), and panel b shows the same analysis obtained from erythrocytes after treatment with external chymotrypsin prior to lysis (lane 2). Although external chymotrypsin is known to cleave AE1 into an N-terminal 61 kDa proteolysis product (Ch61) and a C-terminal 39 kDa proteolysis product (Ch39), the smaller fragment was not detected by Coomassie Blue staining, possibly because it is highly glycosylated (*28*). Panel c shows the density profile obtained from an autoradiogram of [^{14}C]-TIDS-labeled erythrocytes (lane 3). Quantification of the densitometric scan by integration indicated that approximately 45% of the ligand was associated with AE1, 15% with glycophorin A (GPA) ($M_{w,app}$ = 93 kDa), and the rest with undetermined components of the erythrocyte membrane. Proteolytic removal of these components with trypsin yielded membranes where greater than 90% of the radioactivity was associated with AE1 (panel d). The autoradiogram pattern obtained after treatment of [^{14}C]TIDS-labeled erythrocytes with external chymotrypsin indicates that Ch61 contains the site(s) of covalent reaction with the ligand (panel e). Preincubation of whole erythrocytes with DIDS blocked [^{14}C]-TIDS labeling of AE1 (data not shown).

The molar stoichiometry of inhibitor binding to AE1 was (1.2 ± 0.4):1, derived from three separate experiments and assuming a copy number of 1.2 × 10^6 AE1 molecules per cell (*38*). The fraction of label associated with lipid was less than 1% of the total amount of inhibitor bound to the membrane.

Inhibition of Sulfate Equilibrium Exchange in Intact Erythrocytes by TIDS. Figure 2a presents representative data obtained from measuring the rate of sulfate equilibrium exchange in whole erythrocytes with increasing concentrations of TIDS. From such measurements, Hill plots were constructed to determine the concentration of inhibitor required for half-maximal inhibition (IC_{50}) and to assess the cooperativity of ligand binding (Figure 2b). Kinetic analysis of erythrocytes, erythrocytes after extracellular trypsin diges-

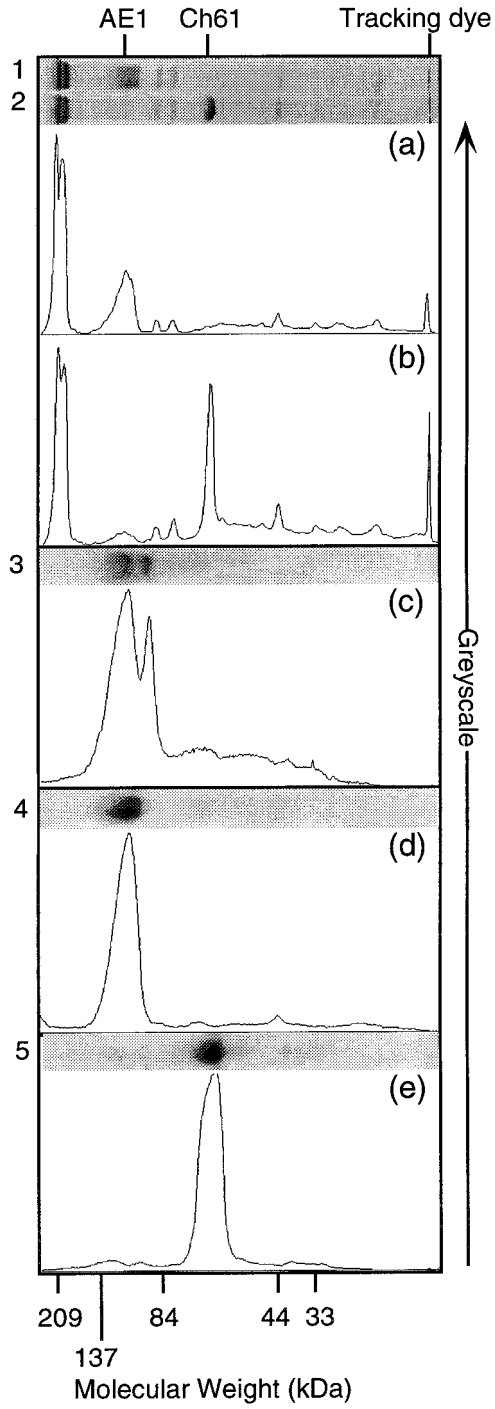

FIGURE 1: SDS (10%)−polyacrylamide gel electropherogram and autoradiogram analysis of TIDS binding to AE1. Coomassie-stained gel and densitometry profiles of ghost membrane [lane 1 and (a) 10 μg of total protein loaded] and membrane after treatment with external chymotrypsin [lane 2 and (b) 10 μg of total protein loaded]. Autoradiograms and densitometry profiles of [^{14}C]TIDS-labeled ghost membranes [lane 3 and (c) 10 μg of total protein loaded], membranes after external treatment with trypsin [lane 4 and (d) 50 μg of total protein loaded], and membranes after external treatment with chymotrypsin [lane 5 and (e) 50 μg of total protein loaded].

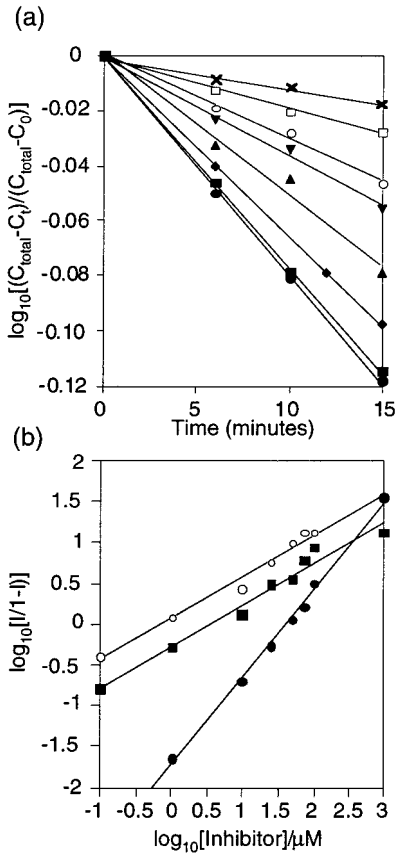

FIGURE 2: Representative sulfate equilibrium exchange data obtained from whole cells in the presence of 0 (●), 1 (■), 10 (◆), 25 (▲), 50 (▼), 75 (○), 100 (□), and 1000 μM (×) TIDS (a). Hill plots derived from sulfate equilibrium exchange measurements for TIDS binding to whole cells (●), as well as TIDS binding to cells after either external trypsin (○) or external chymotrypsin (■) proteolysis (b). Analysis was performed on data derived from three separate experiments.

tion, and erythrocytes after extracellular chymotrypsin digestion yielded initial rates of sulfate equilibrium exchange of $(7 \pm 2) \times 10^{-3}$, $(6 \pm 4) \times 10^{-3}$, and $(9 \pm 3) \times 10^{-3}$ min^{-1}, respectively. Inhibition of sulfate equilibrium exchange by TIDS was characterized by IC_{50} values of 40 ± 11, 0.71 ± 0.48, and 3.4 ± 2.2 μM and Hill coefficients of 1.10 ± 0.06, 0.51 ± 0.01, and 0.51 ± 0.11 for erythrocytes, erythrocytes after extracellular trypsin digestion, and erythrocytes after extracellular chymotrypsin digestion, respectively.

Effect of TIDS Binding on the Thermal Denaturation of AE1. The effect of bound TIDS upon the thermodynamic stability of AE1, as determined by differential scanning calorimetry, was compared to those of both native erythrocyte ghost membranes and DIDS-labeled membranes (Figure 3). All three samples were treated with external trypsin prior to ghost membrane preparation to remove ligand bound to components of the erythrocyte membrane other than AE1. The temperature at which the calorimetric C transition of AE1 denaturation in unlabeled erythrocyte ghosts occurred was determined to be 66 ± 1 °C (panel a). Binding of TIDS to erythrocyte ghosts induced a 4 ± 1 °C rise in the temperature of the C transition (panel b), whereas labeling with DIDS induced a 10 ± 1 °C increase in the C transition temperature relative to that of the unlabeled membrane (panel c).

Evaluation of the Orientation of Erythrocyte Ghost Membranes by ^{31}P NMR and Thin Section Electron Microscopy. To provide a reference spectrum for comparison to spectra derived from oriented membrane samples, the static powder ^{31}P NMR spectrum of a TIDS-labeled and trypsin-treated erythrocyte ghost membrane dispersion was obtained (Figure 4, upper spectrum). This spectrum is diagnostic of a liquid crystalline lipid phase with a low-field shoulder $\sigma_{||}'$

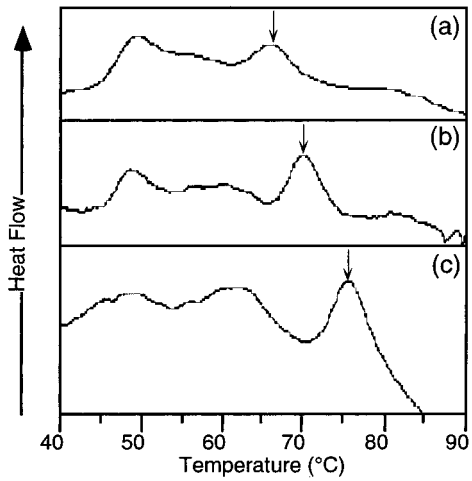

FIGURE 3: Differential scanning calorimetry thermograms of ghost membranes (a), where the C-transition temperature characterizing AE1 membrane domain denaturation (↓) was compared to C-transition temperatures obtained for both the TIDS−AE1 complex (b) and the DIDS−AE1 complex (c). In all samples, erythrocytes were treated with external trypsin prior to membrane preparation.

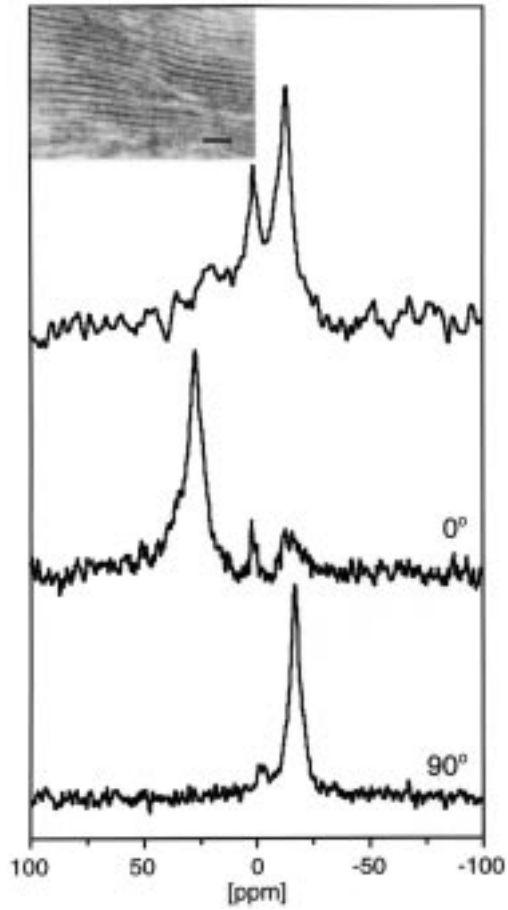

FIGURE 4: ^{31}P static NMR spectra recorded at ambient temperature of fully hydrated unoriented ghost membranes (upper spectrum) and macroscopically aligned membranes with the external magnetic field either parallel (middle 0° spectrum) or perpendicular (lower 90° spectrum) to the membrane normal. Thin section electron micrograph of aligned membranes, sectioned perpendicular to the plane of the membrane (inset). The bar represents 100 nm. In all samples, erythrocytes were treated with external trypsin prior to lysis.

at 27.5 ppm and a high-field peak $\sigma_{\perp}'$ at −12.5 ppm. The measured chemical shift anisotropy (CSA = $\Delta\sigma$), defined as $\Delta\sigma = \sigma_{||}' - \sigma_{\perp}'$, was 40.0 ppm. An additional resonance observed at 1.5 ppm characterizes near-isotropic motions and may originate from a non-bilayer lipid phase.

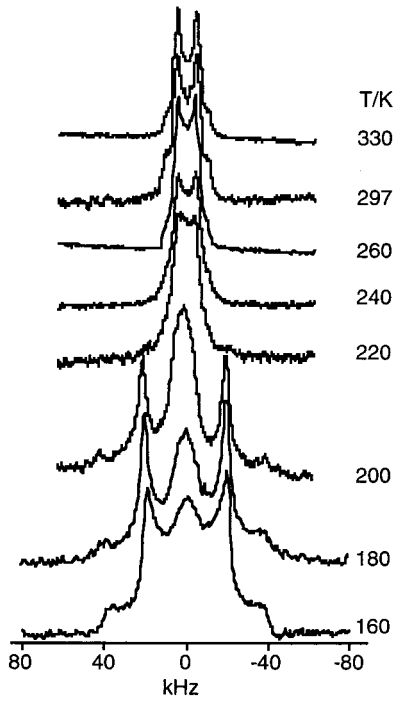

FIGURE 5: Temperature-dependent deuterium quadrupolar spectra of crystalline [$^2H_9$]TIDS. Spectra were averaged over 1024 acquisitions and processed with 100 Hz line broadening.

Macroscopic membrane orientation was achieved by isopotential spinning followed by controlled partial dehydration of the sample by incubation at 81% humidity over a saturated $(NH_4)_2SO_4$ solution. The static ^{31}P NMR spectrum at 0 ° sample inclination exhibited a large single peak at 27.6 ppm which shifted to −12.7 ppm at 90° orientation. The CSA of this oriented sample was measured at 40.3 ppm, close to that obtained for the powder ^{31}P NMR erythrocyte ghost sample. Two further peaks were observed in the 0° spectrum. The resonance at −12.7 ppm, which characterizes unoriented material, represented 10% of the total phosphorus signal. The other resonance at 2.6 ppm accounted for 3% of the total phospholipid. Oriented membrane samples examined by thin section electron microscopy indicated that extensive alignment of ghost membrane is rarely interrupted by unoriented fragments, confirming the static ^{31}P NMR measurements (Figure 4, inset).

Static ^2H NMR Spectra of Solid [$^2H_9$]TIDS. The polycrystalline powder ^{2}H NMR spectrum of the deuterated stilbene disulfonate was recorded as a function of temperature to provide reference spectra with which the ^{2}H NMR spectral line shapes of inhibitor bound to AE1 in erythrocyte ghost membranes could be compared (Figure 5). At 330 K, an axially symmetric powder pattern is characterized by a $\Delta\nu_q$ of 3.7 ± 1.0 kHz. Reducing the temperature to 260 K increased the measured quadrupolar splitting ($\Delta\nu_q$ = 8.5 ± 1.0 kHz), indicating a reduction in motional averaging of $\Delta\nu_q$ compared to those of spectra recorded at higher temperatures. The spectral intensity in the central region of the spectrum also increased at 260 K, characteristic of intermediate motions. At 200 K, peaks separated by 41 ± 1 kHz characterize fast 3-fold rotational averaging of the

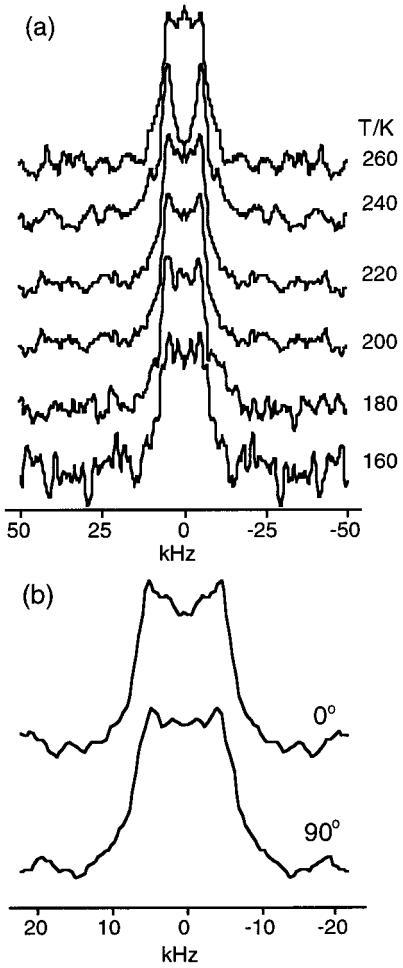

FIGURE 6: Temperature-dependent deuterium quadrupolar spectra of a fully hydrated unoriented erythrocyte ghost membrane sample labeled with [$^2H_9$]TIDS (a). Deuterium quadrupolar spectra at 240 K of oriented [$^2H_9$]TIDS-labeled ghost membrane with the external magnetic field either parallel (upper 0° spectrum) or perpendicular (lower 90° spectrum) to the membrane normal (b). Both samples were prepared from cells treated with external trypsin prior to lysis and contained 100 mg of total protein. Spectra were averaged over 60 000 acquisitions and processed with 1 kHz line broadening.

$N^+(CD_3)_3$ rotor about a single axis. As the temperature is further reduced, the intensity of the central peak diminishes as intermediate motions are arrested.

Static ^2H NMR Spectra and Longitudinal Relaxation Analysis of [$^2H_9$]TIDS Bound to AE1. Figure 6a shows the temperature-dependent static deuterium NMR from an unoriented fully hydrated ghost membrane sample labeled with [$^2H_9$]TIDS and treated with extracellular trypsin prior to cell lysis. At 260 K, the line shape is characterized by a $\Delta\nu_q$ of 9.8 ± 1.0 kHz, with the spectral intensity centered around 0 kHz from intermediate motion. At 240 K, a loss in spectral intensity derived from intermediate motions was observed compared to that of the spectrum acquired at 260 K. At 220 K, the spectral line shape characterized by a $\Delta\nu_q$ of 9.5 ± 1.0 kHz became more complex as intermediate motions are reintroduced with concomitant increases in spectral intensity centered around 0 kHz. As the temperature is decreased further, very little change in line shape is observed, although the integrated spectral intensity is reduced due to homogeneous T_2 processes.

Figure 6b shows the deuterium spectra recorded at 240 K and two different sample inclinations of an oriented partially dehydrated ghost membrane sample labeled with [$^2H_9$]TIDS and treated with extracellular trypsin prior to cell lysis. The spectra obtained from this oriented sample inclined at 0 and 90° to the external magnetic field were characterized by quadrupolar splittings of 9.6 ± 1.0 and 8.8 ± 1.0 kHz, respectively. Since all spectra were processed with a line broadening of 1.0 kHz, the observed differences in the quadrupolar splittings at the two sample inclinations were considered insignificant. Furthermore, no changes in spectral line shape or quadrupolar splitting values were observed from inclining the sample at either 30 or 60° relative to the magnetic field (data not shown).

Longitudinal relaxation measurements, described by the relaxation constant T_1, quantified reporter group dynamics. A T_1 value of 16.2 ± 0.1 ms obtained for the ligand dissolved in deuterium-depleted water compares to a T_1 value of 7.40 ± 0.04 ms for the solid ligand at 260 K. For TIDS bound to AE1 in ghost membranes, a T_1 value of 16.30 ± 0.07 ms was obtained at the same temperature, which was indistinguishable from inhibitor motions in deuterium-depleted water.

DISCUSSION

Covalent Modification of AE1 by TIDS. The observations that DIDS blocks subsequent labeling of AE1 by TIDS, that the covalent site of TIDS reaction with AE1 is on the same Ch61 domain as the DIDS reaction site (*39*), and that both TIDS and DIDS bind with a 1:1 molar stoichiometry all indicate that TIDS and DIDS share the same site of covalent attachment. The lysine residue which reacts with DIDS is either Lys_{542} exclusively or both Lys_{542} and Lys_{539}, and these are likely to be the same residues which react with TIDS (*40*). However, distinct but allosterically linked sites for TIDS and DIDS labeling of AE1 cannot be discounted.

Inhibition of AE1 by TIDS. Comparing TIDS inhibition of AE1 with previous studies using other stilbene disulfonates provides some insight into how the chemical properties of these ligands govern their interaction with erythrocytes (*1*, *41*). The specificity of TIDS binding to AE1 in whole cells is less than previously observed for more hydrophobic stilbene disulfonates (*3*), indicating that hydrophobicity correlates with ligand specificity. The increased inhibitory potency of more hydrophobic stilbene disulfonates may therefore be a consequence of this increased specificity for AE1 in whole cells. The influence of electrophilicity was examined by comparing the inhibitory potencies of TIDS with that of the closely related compound 4-nitro-4′-isothiocyanostilbene-2,2′-disulfonic acid (NIDS). The Hammett σ constant for $N^+(CH_3)_3$ ($\sigma^{\rho}_{N^+(CH_3)_3} = 0.96$) is greater than that for NO_2 ($\sigma^{\rho}_{NO_2} = 0.81$), indicating that TIDS is more electrophilic than NIDS (*42*). The IC_{50} value for TIDS in trypsin-treated cells is less than that for NIDS in whole cells (*1*), suggesting that increased inhibitory potency is related to increased electrophilicity (*41*). However, comparison of the IC_{50} values for TIDS in trypsin-treated cells with NIDS in whole cells assumes a similar specificity of both ligands for AE1 in the two systems. This assumption seems justified since NIDS is more hydrophobic than TIDS and hydrophobicity seems to correlate with ligand specificity for AE1 in whole cells.

Cooperativity of TIDS Binding to AE1. The finding that negative cooperativity of TIDS binding is induced only after

trypsinization of intact cells, together with previous observations where the negative cooperativity of H_2DIDS binding is observed only for purified AE1 (*41*, *43*), supports a model where trypsin sensitive proteins modulate AE1 allostery. A likely candidate for modulation of AE1 allostery is GPA, which is found in similar abundance in the red blood cell (*44*). Previous studies support a GPA−AE1 adduct stabilized by electrostatic interactions between charged groups in exofacial loops (*44*). If it is assumed that complexation of GPA with AE1 modulates the monomer−monomer interface within the AE1 dimer, then disruption of the charge interaction between GPA and AE1 may also affect cooperativity of stilbene disulfonate binding. Trypsinization may dissociate the GPA−AE1 complex by releasing charged residues from GPA that interact with AE1. A high salt level may also dissociate the GPA−AE1 adduct, and a salt dependence of stilbene disulfonate cooperativity has previously been reported (*6*, *17*, *45*).

Conformational Perturbation of AE1 by TIDS. Previous thermodynamic analysis of stilbene disulfonate binding revealed that initial ligand binding stabilized AE1 to a small extent, whereas subsequent relocation of these probes to a rigid, hydrophobic cleft within the protein interior and close to the cytoplasmic surface of the membrane was concomitant with more significant protein stabilization (*4*, *6*, *7*). The greater thermodynamic stability of the DIDS−AE1 complex compared to that of the TIDS−AE1 adduct may therefore indicate a minimal degree of relocation of TIDS into the protein interior compared to that of DIDS. The difference between DIDS and TIDS is replacement of an isothiocyano group by a quaternary ammonium group. Introduction of a cationic functional group may arrest relocation of the ligand to the proposed hydrophobic site near the cytoplasmic surface of the membrane (*6*).

Static ^{2}H NMR Characterization of the TIDS−AE1 Complex. The observed lack of deuterium line shape dependence on sample inclination in macroscopically oriented samples may be due to a large distribution of membrane normals resulting in a large distribution of axes describing the orientation of the stilbene disulfonate with respect to the external magnetic field. Alternatively, the dynamics of the probe bound to AE1 may be described by a large amplitude wobbling or precessional motion. To differentiate between these two possibilities, ^{2}H NMR line shape simulations were used to determine if the distribution of membrane normals is sufficient to average the predicted deuterium line shape dependence on sample inclination (*35*). These ^{2}H NMR line shape simulations modeled the *N*-methyl rotor undergoing fast rotation about both the C_3 and C_3' axes, as well as fast motional averaging about a third axis at an angle of 27° from the C_3 axis. Motional averaging about this third axis was required to account for the observed $\Delta\nu_q$ of 9.8 ± 1.0 kHz obtained from the powder membrane sample, less than the expected value of 14 kHz for an *N*-methyl rotor undergoing fast rotation about both the C_3 and C_3' axes only (eq 1). The distribution of membrane normals in oriented membranes was obtained from ^{31}P NMR spectra. By measuring the line width at half-height of the main resonance peak for both the 0 and 90° ^{31}P NMR spectra, and using the relationship $\nu_{CSA} = -^2/_3\Delta\sigma(3\cos^2\theta - 1)/2$, where ν_{CSA} ($\theta = 0°$) $= -\sigma_{||}'$ and ν_{CSA} ($\theta = 90°$) $= -\sigma_{\perp}'$, we obtained values of ±16° and ±18°, respectively, for the distribution of phospholipid motional axes about some mean orientation (*46*). Also, from direct spectral simulation of the ^{31}P NMR spectra, including consideration of the known differences in CSA for both phosphatidylcholine and phosphatidylethanolamine lipids, the distribution of phospholipid motional axes about some mean orientation was estimated to be ±20° (*32*). The ^{2}H line shape spectral simulations indicated that even with a value for the distribution of phospholipid motional axes of ±20°, the simulated spectra were characterized by maximum and minimum quadrupolar splittings of 15.5 and 8.5 kHz, respectively. We therefore conclude that the observed lack of ^{2}H NMR line shape dependence on sample inclination indicates that the *N*-methyl rotor motions cannot be described by simple fast motional averaging about the C_3 and C_3' axes, as well as a third axis at an angle of 27° from the C_3 axis. Instead, the lack of ^{2}H NMR line shape dependence on sample inclination is more likely due to a wobbling or precessional motion of the ligand (Figure 7).

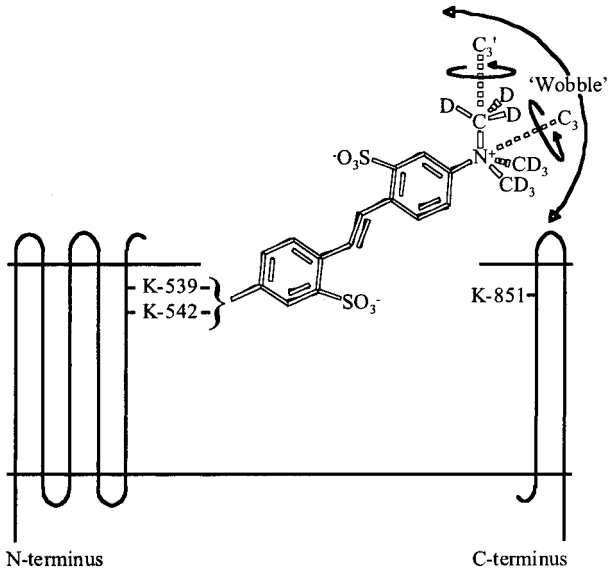

FIGURE 7: Model depicting TIDS bound to AE1 proposed on the basis of the interpretation of both calorimetric and ^{2}H NMR analyses of the ligand−protein complex. Please see the Discussion for details.

Other observations indicate that the ligand is in an aqueous environment and not translocated to the interior of the protein. First, a $\Delta\nu_q$ of ~2 ± 1 kHz at 277 K (data not shown) contrasts with a $\Delta\nu_q$ of 9.8 ± 1.0 kHz at 260 K, indicating that the dynamics of TIDS bound to AE1 is influenced by freezing the sample. Large-amplitude motions characterizing TIDS bound to AE1 at 277 K were also observed for deuterated amino acids defining extracellular loops of bacteriorhodopsin, which contrasted with restricted rotation of labeled amino acids incorporated into transmembrane segments (*47*, *48*). The large-amplitude motions of TIDS observed above the freezing point of water may define a large distribution of axes describing the spatial orientation of TIDS in the frozen state. The lack of ^{2}H NMR line shape dependence on sample inclination in oriented samples may be due to this proposed spatial distribution of the ligand. Second, T_1 measurements show that reporter group dynamics of the inhibitor bound to the membrane are indistinguishable from the dynamics of the inhibitor in solution but distinct from dynamics of the solid ligand. These observations support a model where TIDS is in contact with the aqueous phase when bound to AE1, but provide no information about

whether the ligand is exofacially or cytosolically located. However, we propose that TIDS is more likely located at the exofacial membrane surface since (a) stilbene disulfonates bind with high affinity and high specificity only to the outward-facing conformation of AE1 (*27*), (b) a large thermodynamic stabilization of AE1 following binding of TIDS was not observed, indicating that the probe may not be relocated to the interior of the protein or presumably to the cytoplasmic surface (*4*), and (c) other biophysical studies question whether hydrophobic stilbene disulfonates are indeed translocated to the interior of the protein close to the cytoplasmic surface (*9*).

In conclusion, the negative cooperativity of TIDS binding was only revealed after external trypsinization of whole cells, suggesting that in situ monomer−monomer interactions within the dimeric AE1 complex may be modulated by other erythrocyte membrane proteins. Comparison of the inhibitory potency of TIDS with those of other stilbene disufonates suggests that increasing the electrophilicity of these ligands may correlate with increased inhibitory potency. Increasing the hydrophobicity of stilbene disulfonates increases ligand specificity for AE1 but may not be important in the mechanism of inhibition. Finally, both calorimetric and solid state ^{2}H NMR analyses support a model for the TIDS−AE1 complex where TIDS is not relocated to the interior of the protein. Since TIDS is a potent inhibitor of AE1, then ligand relocation to the protein interior is not required for inhibition of anion exchange.

ACKNOWLEDGMENT

We thank Dr. F. Riddell (Stirling University, Stirling, Scotland) for use of the NMR spectrometer at Stirling University. Sulfate equilibrium exchange was performed under the guidance of Professor C. Ellory (Department of Physiology, University of Oxford, Oxford, U.K.).

REFERENCES

1. Cabantchik, Z. I., and Greger, R. (1992) *Am. J. Physiol. 262* (Part 1), 803−827.
2. Passow, H. (1986) *Rev. Physiol. Biochem. Pharmacol. 103*, 61−203.
3. Cabantchik, Z. I., and Rothstein, A. (1974) *J. Membr. Biol. 15*, 207−226.
4. Verkman, A. S., Dix, J. A., and Solomon, A. K. (1983) *J. Gen. Physiol. 81*, 421−449.
5. Dix, J. A., Verkman, A. S., and Solomon, A. K. (1986) *J. Membr. Biol. 89*, 211−223.
6. Rao, A., Martin, P., Reithmeier, R. A. F., and Cantley, L. C. (1979) *Biochemistry 18*, 4505−4516.
7. Thevenin, B. J.-M., Bicknese, S. E., Verkman, A. S., and Shohet, S. B. (1996) *Biophys. J. 71*, 2645−2655.
8. Wojcicki, W. E., and Beth, A. H. (1993) *Biochemistry 32*, 9454−9464.
9. Knauf, P. A., Law, F.-Y., and Atherton, S. J. (1999) *Biophys. J. 76*, A233.
10. Schopfer, L. M., and Salhany, J. M. (1995) *Biochemistry 34*, 8320−8329.
11. Falke, J. J., and Chan, S. I. (1986) *Biochemistry 25*, 7895−7898.
12. Schnell, K. F., Elbe, W., Kasbauer, J., and Kaufmann, E. (1983) *Biochim. Biophys. Acta 732*, 266−275.
13. Frohlich, O. (1982) *J. Membr. Biol. 65*, 111−123.
14. Passow, H., Wood, P. G., Lepke, S., Muller, H., and Sovak, M. (1992) *Biophys. J. 62*, 98−100.
15. Wang, D. N., Kuhlbrandt, W., Sarabia, V. E., and Reithmeier, R. A. F. (1993) *EMBO J. 12*, 2233−2239.
16. Boodhoo, A., and Reithmeier, R. A. F. (1984) *J. Biol. Chem. 259*, 785−790.
17. Macara, I. G., and Cantley, L. C. (1981) *Biochemistry 20*, 5095−5105.
18. Torchia, D. A. (1984) *Annu. Rev. Biophys. Bioeng. 13*, 125−144.
19. Penner, G. H., Polson, J. M., Daleman, S. I., and Reid, K. (1993) *Can. J. Chem. 71*, 417−426.
20. Seelig, J. (1977) *Q. Rev. Biophys. 10*, 353−418.
21. Spiess, H. W., and Sillescu, H. (1981) *J. Magn. Reson. 49*, 107−121.
22. Cross, T. A. (1997) *Methods Enzymol. 289*, 672−696.
23. Ulrich, A. S., Watts, A., Wallat, I., and Heyn, M. P. (1994) *Biochemistry 33*, 5370−5375.
24. Salhany, J. M. (1996) *Cell. Mol. Biol. (Paris) 42*, 1065−1096.
25. Maddy, A. H., (1964) *Biochim. Biophys. Acta 88*, 390−399.
26. Sommer, H. Z., Lipp, H. I., and Jackson, L. L. (1971) *J. Org. Chem. 36*, 824−828.
27. Kampmann, L., Lepke, S., Fasold, H., Fritzsch, G., and Passow, H. (1982) *J. Membr. Biol. 70*, 199−216.
28. Dzandu, J. K., Deh, M. E., and Wise, G. E. (1985) *Biochem. Biophys. Res. Commun. 126*, 50−58.
29. Dodge, J. T., Mitchell, C., and Hanahan, D. J. (1963) *Arch. Biochem. Biophys. 100*, 119−130.
30. Laemmli, U. K. (1970) *Nature 227*, 680−685.
31. Hamaguchi, H., and Cleve, H. (1972) *Biochem. Biophys. Res. Commun. 47*, 459−464.
32. Gröbner, G., Taylor, A. M., Williamson, P. T. F., Choi, G., Glaubitz, C., Watts, J. A., de Grip, W. J., and Watts, A. (1997) *Anal. Biochem. 254*, 132−138.
33. Ge, M., Budil, D. E., and Freed, J. H. (1994) *Biophys. J. 67*, 2326−2344.
34. Davis, J. H., Jeffrey, K. P., Bloom, M., Valic, M. F., and Higgs, T. P. (1976) *Chem. Phys. Lett. 42*, 390−412.
35. Ulrich, A. S., and Watts, A. (1993) *Solid State Nucl. Magn. Reson. 2*, 21−36.
36. Ulrich, A. S., Heyn, M. P., and Watts, A. (1992) *Biochemistry 31*, 10390−10399.
37. Markwell, M. A., Haas, S. M., Bieber, L. L., and Tolbert, N. E. (1978) *Anal. Biochem. 87*, 206−210.
38. Steck, T. L. (1978) *J. Supramol. Struct. 8*, 311−324.
39. Lepke, S., Fasold, H., Pring, M., and Passow, H. (1976) *J. Membr. Biol. 29*, 147−177.
40. Garcia, A. M., and Lodish, H. F. (1989) *J. Biol. Chem. 264*, 19607−19613.
41. Barzilay, M., Ship, S., and Cabantchik, Z. I. (1979) *Membr. Biochem. 2*, 227−254.
42. Carey, F. A., and Sundberg, R. J. (1990) in *Advanced Organic Chemistry, Third Edition, Part A: Structure and Mechanisms*, p 201, Plenum Press, New York.
43. Boulter, J. M., Taylor, A. M., and Watts, A. (1996) *Biochim. Biophys. Acta 1280*, 265−271.
44. Bruce, L. J., Ring, S. M., Anstee, D. J., Reid, M. E., Wilkinson, S., and Tanner, M. J. (1995) *Blood 85*, 541−547.
45. Dix, J. A., Verkman, A. S., and Solomon, A. K. (1979) *Nature 282*, 520−522.
46. Hing, A. W., Adams, S. P., Slibert, D. F., and Norberg, R. E. (1990) *Biochemistry 29*, 4144−4156.
47. Keniry, M. A., Gutowsky, H. S., and Oldfield, E. (1984) *Nature 307*, 383−386.
48. Keniry, M. A., Kintanar, P., Smith, R. L., Gutowsky, H. S., and Oldfield, E. (1984) *Biochemistry 23*, 288−298.

BI990618P